Journal of Materials Chemistry C

Accepted Manuscript

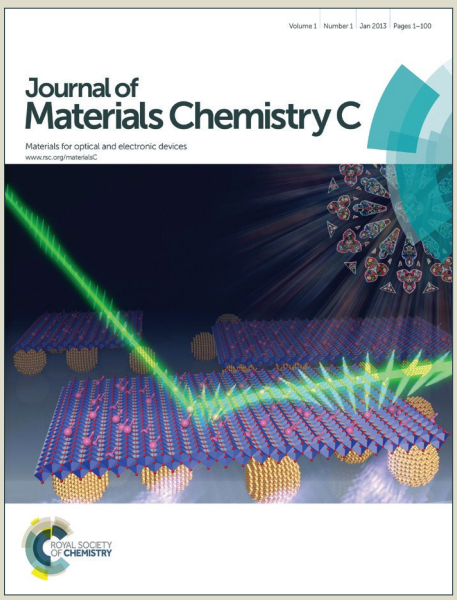

ROYAL SOCIETY OF CHEMISTRY

www.rsc.org/materialsC

Vapor-enhanced covalently bound ultra-thin films on oxidized surfaces for enhanced resolution imaging

Kexin Jiao, Chuanhong Zhou, Nathalie Becerra-Mora, Jared Fiske, Punit Kohli*

Department of Chemistry and Biochemistry

Southern Illinois University

Carbondale, IL 62901

*pkohli@chem.siu.edu

ABSTRACT

Vapor-phase covalently bound siloxane thin films of various functionalities on a variety of surfaces, including glass, aluminum, and polyester, was demonstrated in one-step process. A few nanometers thick siloxane films deposited on surfaces through vapor-phase using different inert polydimethylsiloxanes (PDMS)without the use of solvent, initiator, or a crosslinking agent. Functional PDMS - fluoro-polysiloxane (F-PDMS) and amino-polysiloxane (A-PDMS) were also coated on glass substrates providing functional surfaces for patterned array of microlenses (MLs) for near-field imaging applications. We call our siloxane film deposition method SOLVED which refers to **S**il**o**xane-bound **L**ayers through **V**apor **E**nhanced **D**eposition. Our ellipsometry data on the PDMS SOLVED surfaces indicated the film thickness was 6.5±0.3 nm. The siloxane-surface binding was thermally-activated reaction with an apparent activation energy of ~11 kcal/mol. Our optical spectroscopic X-ray photoelectron spectroscopy (XPS) and Fourier-transform Infrared spectroscopy (FTIR) and mass-spectrometry analysis data provided strong evidence that the SOLVED films retained the chemical nature of the polymers used for the coatings. The redox diffusion coefficient of $Fe(CN)_6^{4-/3-}$ species on SOLVED films using cyclic voltammetry (CV) studies were comparable with that of highly packed C_{18}-silane SAMs on ITO-surfaces - implying high quality, uniform, and pinhole defect-free SOLVED coatings on the surfaces. Further, both the CV and water contact angle measurements indicated the photostability of SOLVED and octadecyltrimethoxysilane (OTMS) self-assembled monolayers (SAMs) films on the ITO substrates was comparable. Unlike bulk-PDMS, our ultra-thin SOLVED films did not exhibit any significant changes in the water contact angle over two weeks. A reproducible and stable hydrophobicity with tunable water contact angles (CAs) between 30° and 97° was obtained through plasma treatment. By selectively removing the SOLVED films through oxygen plasma treatment, we demonstrated the fabrication of self-

assembled aqueous $ZnCl_2$ MLs array. Near-field imaging using MLs yielded much higher spatial resolution than that can be obtained using diffraction-limited wide-field imaging.

Introduction

Modifying solid substrate surfaces without changing their bulk properties is of increasing interest among academics and industries. The surface or interface properties of bulk materials, for example, adhesivity, wettability, functionality, and nano/micro-morphology, can be optimized using application of thin film on the surface.[1] The mono-molecular layer of molecules on metal surface was first reported over 60 years ago.[2] Recently, pioneer work on self-assembled monolayers (SAMs) was reported by groups of Nuzzo and Allara,[3-5] and Whitesides[6]. An authorative review on SAMs by Ulman[7] provides fundamental knowledge and potential applications of SAMs on a variety of surfaces. A wide range of applications of the modified solid substrates including tuning surface wettability,[8-11] functionalization of micro-fluidic device channel,[12,13] grafting for electronics[14] or plasmonic devices,[15] surface protection,[16-18] and particle[19] and biomolecules[20,21] sensing and tuning of the work function for opto-electronic applications[22-25] are reported in the literature. In general, a variety of surfaces including glass, silicon, graphene/graphite,[14,15] carbon nanotubes (CNTs),[26,27] semiconductor materials,[28,29] gold nanoparticles and surfaces,[30,31] and polymer[32-34] can be functionalized using small and large molecules. The mechanism of SAMs formation and the covalent bonding between SAM and substrate is well-known in the literature.[7,35] The reproducibility of the silanized surfaces depends on the quality of silanes, and reaction and processing conditions used in the reactions. For example, the temperature,[36,37] humidity,[38] and solvent of the reaction conditions can affect SAMs formation on the surfaces.[39] Additionally, for enhancing the stability of the silane coatings on the surfaces, a post-polymerization baking step for the formation of siloxane bonds is commonly used. Many silanes (especially, chloro- and bromo-silanes) are highly moisture sensitive requiring inert atmosphere for their storage and reaction with the surfaces.

For a long time in the literature, the siloxane polymers were considered to be “unreactive” toward the inorganic surfaces at low temperature but recent studies have shown that siloxane polymers can chemically react with metal-oxide surfaces.[40-44] Recently, fluoro-, amino-, and phenyl-functional groups containing linear siloxanes were covalently bound to metal-oxide surfaces through bulk polymer fluid-solid surface phase reaction.[41,44,45] The groups of McCarthy, Litvinov, and Fadeev demonstrated that the siloxane-surface chemical binding is dependent upon

the molecular weight of the polymer, and temperature, water content, and time of the reaction.[41-44] In another recent report, "loose" siloxane molecules present in the thermally cured siloxane polymers were transferred and covalently reacted with clean surfaces via solution phase and stamping methods for applications in the surface patterning and lithography.[46-48] Recently, siloxane hydrophobizer was deposited on the surface which stable temperature up to 300°C and pH 2-13[49]. In most of the studies reported in the literature, the inorganic surfaces were in contact with the bulk siloxane fluids during chemical reaction. The investigations involving the reaction of siloxanes with inorganic surface via vapor phase are limited to dimethylsilanediol (MW ~ 92).[50]

In this work, we demonstrate covalently bound ultrathin coatings (comparable thickness with SAMs) of different functionalities on four different surfaces (glass, aluminum, stainless steel, and polyethylene terephthalate (PET)). We utilized commercially-available siloxane polymers in vapor-phase for reaction with the surfaces through a thermal treatment (between 150-300 °C for 15-60 minutes). We refer this deposition as **S**il**o**xane-bound **L**ayers through **V**apor **E**nhanced **D**eposition, abbreviated as SOLVED. The surface was not in contact with the bulk liquid polymer in our studies. Following two hours of sequential sonication in toluene and ethanol, we characterized the SOLVED films using ellipsometry, contact angle, FTIR, XPS, MS, and CV. The apparent activation energy of the siloxane deposition on the glass surfaces was estimated from the water contact angle-temperature dependent Arrhenius plot. The chemical composition of the covalently-bound films on the substrates was confirmed using FTIR, MS, and XPS through the presence of CF_3 and NH vibration peaks for poly(trifluoropropylmethylsiloxane (F-PDMS) and aminoethylaminoproylmethoxysiloxane-dimethylsiloxane copolymer (N-PDMS) SOLVED films respectively. Our XPS analysis suggested that the covalent binding of the siloxane to the surfaces survived relative high temperature (up to 250 ^{o}C) treatment although some oxidation of the functionalized surfaces was also observed in the XPS data. The CV and redox diffusion measurements on the SOLVED films indicated that the photochemical stability of SOLVED films was comparable with that of highly-ordered OTMS SAMs. High refractive index array of $ZnCl_2$ aqueous MLs were fabricated on the patterned SOLVED surfaces for high-resolution imaging in the near-field mode.

Results and Discussion

Fig. 1a shows the general procedure for the preparation of covalently bound coating onto a glass substrate using SOLVED. As received commercial siloxane polymers (PDMS, F-PDMS, and N-PDMS) ~100 μm thick film on a reservoir glass substrate (*R*) were kept ~1-5 mm above a target surface (*T*). This assembly was heated to 150-300°C for 30 min in dark. The target surface was cooled down to room temperature and was sonicated sequentially in toluene and ethanol for ~1-2 hour each to wash weakly adsorbed molecules away from *T* prior to characterization of the coating.

Ellipsometry studies on SOLVED films. Figure 1a shows spectroscopic ellipsometry (SE) measurements for PDMS coating on a silicon substrate using SOLVED performed at 250°C. SE analysis shows a fast initial increase in the siloxane film thickness with deposition time followed by a plateau thickness of ~8.5 nm. The SE was found to reduce to ~6.5 nm after rigorous sonication of the SOLVED coatings in toluene and ethanol for ~2 hours each (Fig. 1b). Our SE thickness of ~6.5 nm using Sylgard 184 base polymer (~60 kD)[51] without crosslinker and catalyst on silicon wafers is in excellent agreement with Fadeev's estimated thickness of ~8 nm for comparable MW ~52.5 kDa siloxane coating.[42] The ellipsometry thickness sensitivity is a

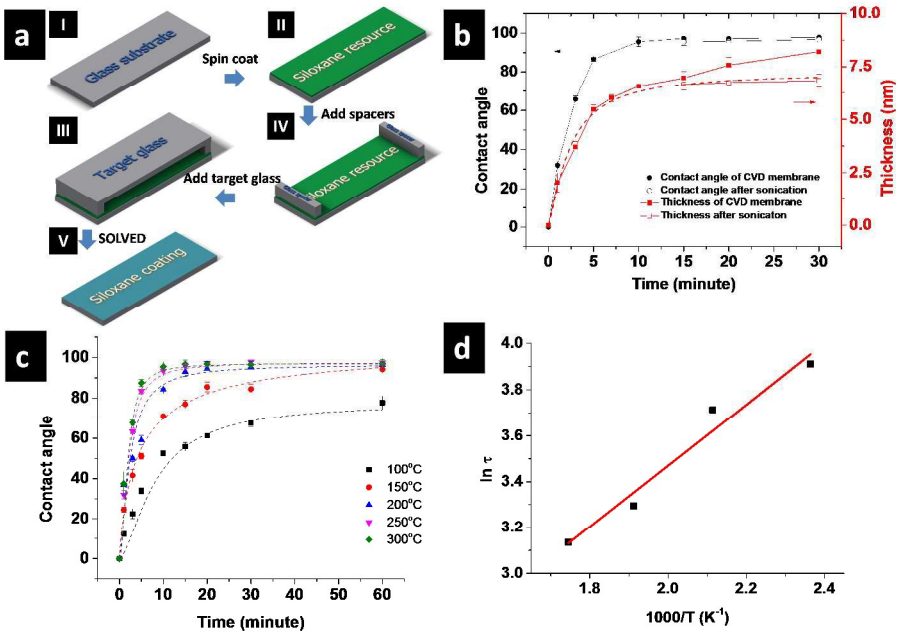

Figure 1. **(a)** Fabrication of covalently-bound siloxane coatings on a glass surface using SOLVED process. (I) A clean glass slide served as a reservoir slide (*R*). (II) Siloxane polymer was spin coated on *R* yielding ~100 μm thick film on the surface. (III) Two spacers (~1-5 mm thick) were placed at two ends of the reservoir glass. (IV) Another clean target glass surface (*T*)

was placed on the two spacers kept on *R*. (V) A covalently bound a few nanometer thick siloxane polymer was resulted on surface *T*. **(b)** Water CA and thickness of the PDMS SOLVED coatings before (solid symbols) and after (hollow symbols) sonication in toluene and ethanol. (c) Water CAs on the SOLVED coated glass surfaces fabricated under different SOLVED temperatures ranging from 100°C to 300°C. A best fit line of the data at five different temperatures is shown in the dashed lines. (d) $\ln \tau_{sat}$-1/T dependence for the PDMS SOLVED coatings on glass surfaces.

fraction of a nanometer, the reduction in SOLVED thickness of ~2 nm after extensive sonication is statistically significant. The reduction in the SE of the SOLVED films after sonication suggested that the SOLVED coatings was consisted of two components – strongly covalent bound siloxanes on the surfaces which remained bound to the surfaces after sonication and a second weakly adsorbed molecules on the surface which were removed with washing. The PDMS SOLVED film thickness of 6-7 nm estimated using Ar sputtering in the XPS experiments was in agreement with the SE thickness results (please see SI for details).

Contact Angle Analysis. The SOLVED functionalization provided low energy surfaces which proved useful for the parameters evaluation and estimation of apparent activation energy for siloxane-surface reaction. The water CA-time dependence data resembled SOLVED film thickness-deposition time trend (Fig. 1b). The water CA increased rapidly with SOLVED deposition time but attained a saturated water CA value of 97° at ~30 minutes for all the deposition temperatures studied in our experiments. Unlike ~2 nm decrease in the SE after sonication, we did not observed any significant decrease in the water CA after sonication suggesting that water CA and SE characterizations provide important but complementary information on our films. The lack of decrease in the water CA suggests that a fraction of molecules were weakly adsorbed at the SOLVED-air interface that were washed off after sonication but did not affect the surface energy. Both the water CA and SE thickness measurements after sonication of the SOLVED coatings confirmed that the SOLVED coatings were strongly bound to the surface. These observations are in agreement with previous reports in the literature.[41-44] Interestingly, the water CA~97° for our SOLVED coated surfaces was smaller than those observed in the previous studies ($\geq$104°) and that of water CA on the bulk PDMS films as well.[41,50] Further, our control experiments where the PDMS SOLVED films were deposited onto glass surfaces in an argon atmosphere showed water CA of ~103.5° in agreement

with literature.[52] The decrease in the water CA for the SOLVED films deposited in air is attributed to slight oxidation of the SOLVED films that resulted in increase of surface energy of the SOLVED films. The oxidation of the SOLVED deposited in air is confirmed by both the XPS and the FTIR studies (see below).

Estimation of the apparent SOLVED activation energy. Figure 1c portrays the temperature-dependent water CA-time studies for the SOLVED coated surfaces. The SOLVED samples were prepared at five different deposition temperatures between 100°C and 300°C, and the water CAs were acquired after rigorous sonication for 2 hrs each in toluene and ethanol. The initial slope difference for water CA-deposition time for different temperature curves relates to the rate of increase in the surface coverage by the siloxane chains on the surfaces. Higher water CA-deposition time slope means faster kinetic of the siloxane-surface reaction. The onset of the water CA plateau was found to be deposition temperature dependent and was used to estimate the apparent activation energy using Arrhenius plot. For the estimation of the apparent activation energy for SOLVED deposition, we assumed full surface coverage by the siloxane molecules attained water CA~97^o. In our experiments, the SOLVED deposition performed at 250°C required only 15 minutes to achieve a water CA value of 97° whereas it required ~55 minutes to attain water CA ~97° when the deposition temperature was 150^{o}C. However, the deposition at 100^{o}C did not attain water CA~97^o suggesting incomplete surface coverage by the siloxane molecules (see below for more details), and this data point was not used for the estimation of the apparent activation energy for the SOLVED process.

We define τ_{sat} as the deposition time for SOLVED coatings which yielded water CA value of 97° (Table 1S). In our case τ_{sat} (=1/k) is a kinetic parameter, where k is the rate constant for the siloxane-surface reaction. E_a ~11 kCal/mol for the siloxane-surface reaction was estimated using Arrhenius equation: $\ln \tau_{sat} = \frac{E_a}{RT}$ (Fig. 1d).[53] As a comparison, the activation energy for the siloxane based reactions varies from 21.4 kCal/mol for KOH catalyzed OH-terminated siloxane to ~176 kcal/mol for trimethylsiloxy-terminated siloxanes.[54] The E_a for the observed siloxane-surface reaction is not a direct comparison with depolymerization of the linear siloxanes. These reactions however points to a wide range of the E_a for siloxane based reactions. The reported thermal depolymerization of the siloxanes is a bulk process where the depolymerization of the chains may occur at multiple sites along the chain through multiple catalytical attacks. The

exact mechanistic nature of the SOLVED process is not known but it is a surface-assisted reaction that may involve one or multiple steps. Low E_a for the SOLVED process suggests that the siloxane covalent binding with surface is an efficient reaction at temperature >150^{o}C yields full-coverage in ~45 minutes.

An important difference in our studies reported in this manuscript compared to the previous studies is that the siloxane deposition at 100^{o}C was performed using bulk siloxane polymers in contact with the hydroxyl groups containing surfaces for extended deposition time ranging from overnight to 24 hours. In the present case, vapor-based siloxane molecules were covalently-bound to the surface for shorter period of time (<1 hour). The surface coverage differences between the present studies and previous results are likely due to time- and concentration-dependence of the siloxane-surface reaction. Assuming the molecular weight of the bulk siloxane polymer ~60 kD, the concentration of siloxane in contact with the surface was ≈0.015 mM. This concentration value is believed to be much larger than that can be achieved in the vapor-phase studies.

FTIR analysis of the SOLVED films. FTIR spectroscopy provides useful information on the molecular orientation and chemical functionality of the films. FTIR analysis on three different SOLVED (PDMS SOLVED, F-PDMS, and N-PDMS) films and bulk-PDMS was performed following sonication in toluene and ethanol for 2 hrs each. All the four samples showed CH stretching (ν_{CH}) and CH bending (δ_{CH}) peaks at ~2961 cm^{-1} and ~1260 cm^{-1} respectively (Fig. 2 and Table S2).[42] The FTIR spectra of the SOLVED films also showed characteristic peaks at1011 cm^{-1} and 1107 cm^{-1} associated with Si-O stretching peak in the cyclic-D_3/D_4 and linear siloxanes respectively (Table 2S and Fig. 1S).[55-57] The low peak intensity ratio of 1011 cm^{-1} to that of 1107 cm^{-1} suggested a relatively small fraction of cyclic siloxanes were incorporation in the SOLVED films. The source of the cyclic siloxanes in the Sylgard 184, F-PDMS, and N-PDMS is thermally decomposition of linear siloxane to cyclic siloxanes. D_3/D_4 are also known to form during thermal treatment of linear siloxane polymers in both inert and air atmospheres.[58] Further, the presence of cyclic siloxanes in the commercial polymers cannot be ruled out.

A strong C-F stretching resonance peak at 1212 cm^{-1} in the F-PDMS FTIR spectrum confirmed the presence of CF_3 function groups in the SOLVED films (blue spectrum in Fig. 2). The presence of CF_3 was also corroborated with the presence of a photoelectron peak at ~293.2 eV that corresponds to the C1s signal from CF_3 in XPS (see below). FTIR spectra for all the

SOLVED films and bulk PDMS also showed a broad-band hydrogen bonded Si-OH stretching peak in the 3100-3400 cm^{-1} region. Further, a peak at ~1640 cm^{-1} attributed to possible carbonyl-like species in N-PDMS films in SOLVED films synthesized at >150°C possibly due to presence of oxidized carbon species in the films. The oxidation of the siloxane coatings is not surprising because the cured PDMS is known to possess an oxidized layer on its surface.[59] Similarly, a lower water CA~97° for the air-grown SOLVED films than that for SOLVED films grown in the argon atmosphere also supported the oxidation argument. Overall, our FTIR data indicated that the SOLVED thin films were primarily composed of chemical species similar to those of starting siloxane polymers, and that the SOLVED films showed some oxidation of the SOLVED films grown in the air.

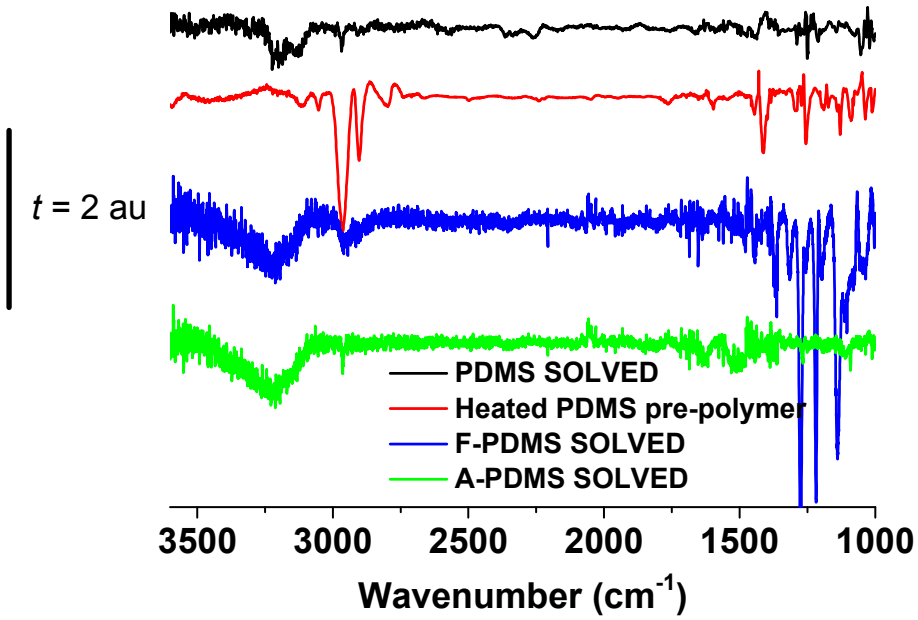

Figure 2. FTIR for SOLVED coating on Si substrate PDMS (black), F-PDMS (blue), N-PDMS (green), and bulk PDMS (red). *t* represents IR transmission % in arbitrary units.

XPS analysis. XPS measurements yielded important chemical and structural information on the SOLVED films because the photoelectron signal in the XPS is sensitive to oxidation state and electron density of the element. For example, the C1s binding energy in a molecule is sensitive to functional groups attached to carbon – the C1s binding energy will be larger for CF_3, carboxylic acid, ester etc. than CH_3, Si-CH_3 cases. All the photoelectron signals in our studies

were referenced to C1s binding energy (BE) of 285 eV for correcting for charging effects of the non-conductive samples.

SOLVED	Origin of the peak	BE (eV)	Atomic Conc. (%)
PDMS	**C1s, total**	**285**	**11.1**
	C1s-H, C1s-Si	285	10.0
	C1s-O	286.5	1.1
	Si2P,total	**99-104**	**28.1**
	Si2p(siloxane)	103.1	4.5
F-PDMS	**C1s, total**	**285-293.2**	**9.3**
	C1s-H, C1s-Si	285	6.8
	C1s-O	286.2	1.5
	C1s-CF_3	293.2	1.0
	F1s	**688.5**	**5.5**
	Si2p	**99**	**34.0**
	Si2p(siloxane)	102.9	2.9
N-PDMS	**C1s, total**	**285-286.1**	**16.4**
	C1s-H, C1s-Si	285	12.3
	C1s-O, C1s-N	287.4	4.1
	N1s, total	**400.2-403.2**	**1.7**
	N1s-C	400.2	1.5
	N1s-O	403.2	0.2
	Si2p	**99**	**34.8**
	Si2p(siloxane)	102.5	2.9

Table 1. XPS analysis of the covalently-bound SOLVED films of three different functional groups.

Tables 1 and 4S provide the BE and atomic concentrations of different elements present in the SOLVED films. XPS measurements provided both the elemental and chemical information in the siloxane polymers bound to the surface. BE peaks at 688.5 eV and 400-403 eV in the XPS analysis verified the presence of fluorine and nitrogen elements in the F-PDMS and N-PDMS films respectively (Fig. 3a). The C1s photoelectron signal for F-PDMS films was composed of three peaks centered at 285 eV, 286.2 eV, and 293.2 eV which correspond to C1s-H/C1s-Si;

C1s-O; and C1s-F_3 species respectively (Fig. 3b). The $I_{C1s\text{-}H}/I_{C1s\text{-}F3}$ ~ 0.22 was slightly smaller than theoretical value of $I_{C1s\text{-}H}/I_{C1s\text{-}F3}$ ~0.25 but was within the error associated with measuring area of weak photoelectron peaks in the spectrum. Here, $I_{C1s\text{-}H}$ and $I_{C1s\text{-}F3}$ refer to C1s photoelectron peaks for C-H_x and C-F_3 respectively. Our XPS data suggested that ~10-15% of the total carbon species, corresponding to the binding energy peak in the 286-287 eV region, in the SOLVED films are oxidized. The presence of oxidized carbon photoelectron signal in all of our siloxane films is not surprising considering that the deposition was performed at relatively high temperature (>100^{o}C) which aided in some partial oxidation of hydrocarbon portion in the films. The oxidation of hydrocarbon side chains of the siloxane also corroborates well with our FTIR analysis where a broad hydrogen-bond containing band in 3200-3500 cm^{-1} region for the SOLVED coatings was observed (Fig. 3). The decrease in the theoretical [F1s]/[C1s] ratio in F-PDMS films from 0.75 to the observed experimental [F1s]/[C1s] ratio value of 0.59 (Table 1) is likely due to oxidation of the SOLVED films which altered the elemental concentrations in the films (see below). Based on larger thermal stability of C-F bonds (bond energy ~110 kcal) compared to C-H bonds (bond energy ~100 kcal), we speculate that the incorporation of oxygen in the F-PDMS SOLVED films is more probable in the C-H containing portion of the films than in the C-F bonds. Another evidence of the oxidation came from the presence of a vibration resonance peak at ~1630 cm^{-1} (possibly C=O stretching vibration peak) in the FTIR spectrum (Fig. 3) and N1s photoelectron peak at BE~403 eV corresponding to NO_x (Fig. 4 and Table 1) confirming oxidized nitrogen species in the N-PDMS SOLVED films.

All the SOLVED films showed a photoelectron peak in 102.5-103.5 eV binding energy region. This peak corresponds to the siloxane specie in the SOLVED films.[60] The Si2p peak is sensitive to the Si bonding to oxygen and carbon elements. For example, the Si2p photoelectron signal in the siloxane with a general formula of -$(CH_3)_m$-Si-$(O)_n$- shifts to higher binding energy with increase in "*n*", that is, when Si is attached to larger number of electronegativity oxygen atoms. Here, $m + n$=4. The backbone of all the PDMS used in our studies possess m=2 and n=2 with a small fraction of the functional amino- and fluoro-siloxanes. $n>m$ means that larger number of Si-O bonds than Si-C bonds in the siloxane polymer. For m=2 and n=2, Si2p peak in the siloxane appeared at ~102.5 eV, whereas it was 103.2 eV for m=1 and n=3 (Fig. 7S). The appearance of a photoelectron peak in 102.5-103.5 eV confirmed the presence of siloxane in the

SOLVED films and that the SOLVED films contained siloxanes with both (m=2 and n=2) and

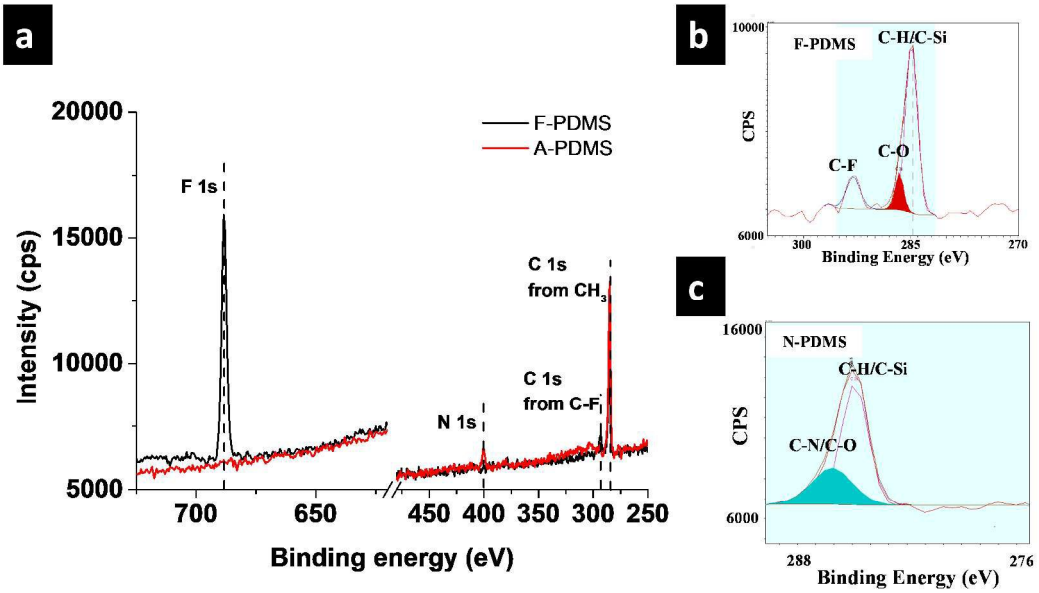

Figure 3. (a) The overlaid XPS survey scans for F-PDMS (black curve) and N-PDMS (red curve) SOLVED coatings on the Si surfaces. Higher resolution XPS scans of the C1s regions for F-PDMS (b) and A-PDMS (c) SOLVED coatings on Si surfaces. The peak-fitting in (b) and (c) was performed using casaXPS. All the peaks were referenced to 285 eV of C_{1s}.

(m=1and n=3). The presence of siloxanes corresponding to the m=1 and n=3 implied some crosslinking in the SOLVED films is also in agreement with superior photostability of the SOLVED films as evident from our CV studies. The degree of crosslinking in our SOLVED films is however not known from these studies.

Mass spectroscopic analysis. The mass spectroscopy analysis for the PDMS SOLVED coating on Si substrate was dominant by an m/z ~ 72.5 peak which corresponds to $C_2H_5SiO^+$ (Fig. 5S). This peak represents a single repeat unit of PDMS.[61] The fraction of larger mass fragments corresponding to longer siloxane chains was small in the SOLVED mass spectra. These observations are consistent with to covalent binding and crosslinking of the siloxanes on the surface which likely reduced the ionization of the larger fragments in the MS.

Tunability of water contact angle using plasma treatment. The water CA tunability of the SOLVED coated glass surfaces was achieved using argon plasma treatment (Scheme 1S). The plasma etching treatment of the SOLVED films exhibited a decrease in the water CA from 97° to a stable value of 30°. The best fitting for the curve in Fig. 4b suggested a linear dependence of CA on plasma etching time. We have not investigated in detail the linear water contact angle-

etching time dependence. However, we attribute the increase of the water CA to the increased number of hydrophilic chemical species at the surface and the silanol groups density at the surface with plasma etching time.[62-64] The water CA of a 5 mm thick bulk thermal-cured PDMS sample treated under the same plasma conditions was found to decrease from 108° to 42° but it was recovered to ~99% of its original water CA value in <10 minutes after keeping in ambient conditions. The rapid hydrophobicity recovery of bulk PDMS surface is due to diffusion of the low molecular weight chains from the bulk of the PDMS to the surface of the PDMS. Low

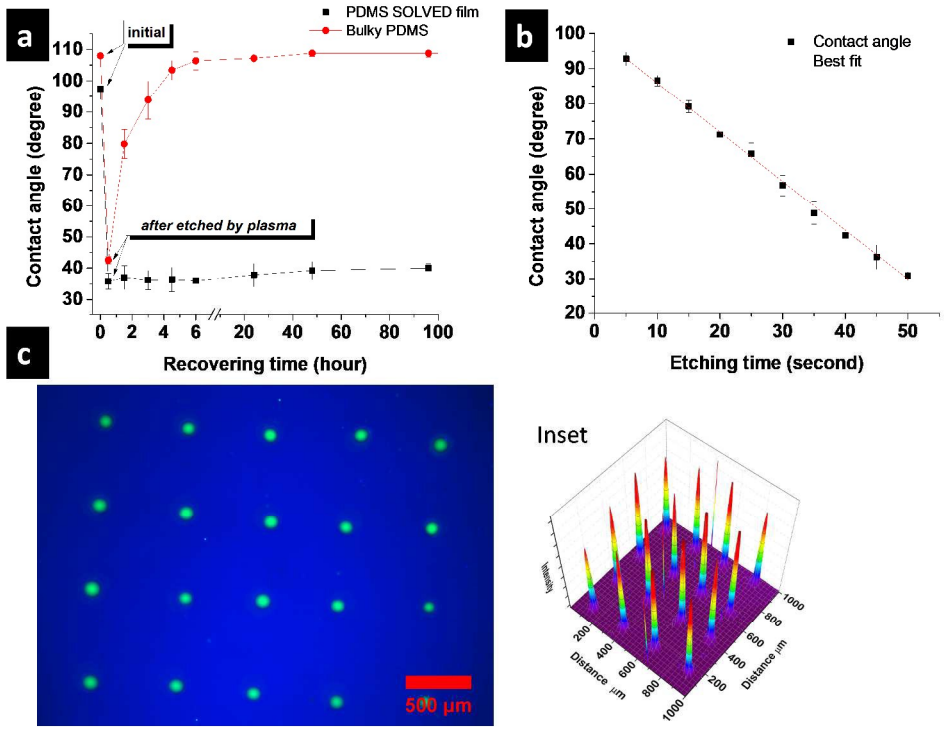

Figure 4. (a) Water CAs on a PDMS SOLVED coated surface (black) and a cured bulk PDMS surface (red). (b) The water CAs of PDMS SOLVED coated glass surface as a function of oxygen plasma etching time. (c) Fluorescence image of fluorescein disodium salt (green color) and 9,10-diphenylanthracene (blue color) on patterned SOLVED coated glass surface. Inset: Intensity analysis for fluorescein emission in (c).

molecular weight hydrophobic oligomers in the thermally cured bulk PDMS are known to diffuse to thermodynamically unstable PDMS-air interface.[52] The diffusion of smaller MW molecules present in the bulk PDMS to the PDMS-air interface is driven by the reduction in the PDMS surface energy to more thermodynamically stable film-air interface. The SOLVED films were thermodynamically stable with no detectable changes in the water CA for at least one week

when kept in the ambient lab conditions. The surface energy stability of the SOLVED films arises due to lack of small molecules in the films. We were also able to tune the water CA of the SOLVED coated surface between 30° and 97° through plasma treatment of the SOLVED films (Fig. 4b and Scheme 1S). Taking advantage of surface energy tunability, we patterned fluorescein (a hydrophilic fluorescence dye) on argon plasma treated F-PDMS SOLVED coated glass slides surrounded by 9,10-Diphenylanthracene (a hydrophobic fluorescence dye) patterns (Figs. 4c and 9S). The fluorescent-patterns were achieved by flushing the plasma-treated surfaces sequentially with 9,10-diphenylanthracene (18 μM) in heptane and aqueous fluorescein (30 μM) solutions. A 3-D fluorescence emission surface plot for the fluorescein emission intensity distribution on a patterned surface shows strong emission only from those hydrophilic windows (inset of Fig. 3c), whereas 9,10-diphenylanthracene emission is dominantly from the hydrophobic area (Fig. 9Sa). The spectrum analysis for two patterned windows revealed contrast values of ~20x and ~5.5x for fluorescein and 9,10-diphenylanthracene respectively (Fig. 9Sb).

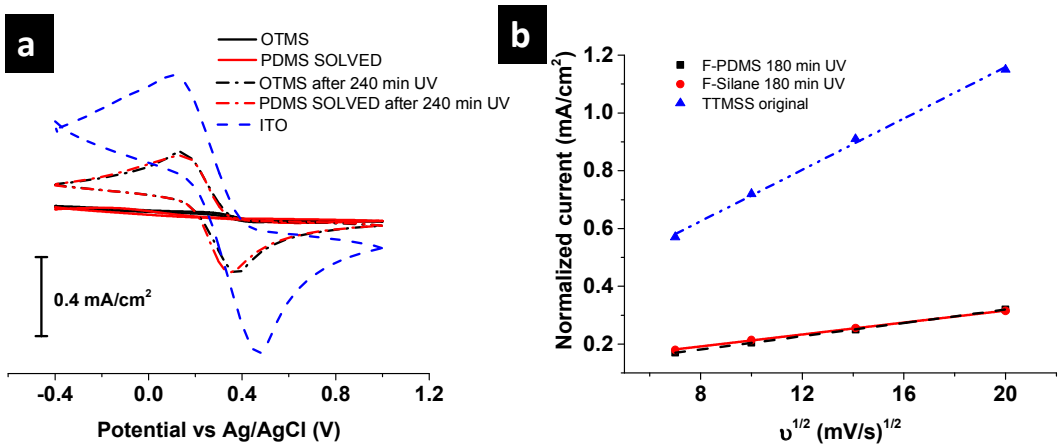

Figure 5. (a) CV spectra for initial (solid curves) and UV exposed (dash dot curves) ITO surface coated SOLVED and OTMS SAMs films. CV for the clean ITO electrode (blue dashed line) is shown as reference. All the CV curves were normalized using electrode area. (b) Comparison of normalized cathodic current-$(\nu)^{1/2}$ on F-PDMS, F-silane, and tetra(trimethylsiloxy)silane (TTMSS) coated ITO electrodes. The diffusion coefficient for the redox species for TTMSS coated electrode was ~16 times larger than those for F-PDMS and F-silane films.

Cyclic voltammetry studies. To evaluate the stability of the SOLVED films, comparison studies of the SOLVED films with the well-studied OTMS SAMs were performed using CV

measurements. These studies also provided information on the packing, pinhole and other defects, and photo-stability of the SOLVED films. We found that the cathodic current (I_{pc}') of $Fe(CN)_6^{3-/4-}$ for the SOLVED films (without UV treatment) was comparable to well-studied OTMS and fluorinated SAMs films on ITO electrodes. Comparable diffusion coefficients of $Fe(CN)_6^{3-/4-}$ were obtained for the SOLVED and SAMs coated electrodes (Fig. 5c). We define $Hydrophilic\ coverage = \frac{I_{pc}'}{I_{pc}^{0}}$ for evaluating the photostability of the coatings examined in our experiments. Here, I_{pc}' and I_{pc}^{0} represent the cathodic current per unit area for the SOLVED films with and without UV exposure respectively. I_{pc}' was estimated by using Eq. 1:

$$I_{pc}' = (2.69\times10^{5})\,n^{3/2}\,AD^{1/2}\nu^{1/2}C_{ox} \qquad \text{Eq. 1}$$

where I_{pc}' is normalized cathodic current. n, A, D, ν and C_{ox} are the number of electrons transferred in the redox reaction, the electroactive surface area of ITO electrode (cm^2), diffusion coefficient of redox species (cm^2s^{-1}), potential scan rate (Vs^{-1}), and the bulk concentration of the redox (mol cm^{-3}) in the solution respectively.

The UV exposure dose for all the films (both SOLVED and SAMs) showed a decrease in the water CA and an increase in the I_{pc}' (Fig. 5). The *Ipc'* values for the SOLVED and SAMs films were comparable to one another but were ~16 times smaller than uncoated ITO bare surfaces (Fig. 8S). Even after irradiation of the SOLVED films with the UV light (254 nm, intensity ~0.5 mW/cm^2) for 4 hours, the I_{pc}' values remained three times lower than that for the bared electrodes suggesting high photostability of the SOLVED films. The defects in the SOLVED coatings were further evaluated by varying the scan rate in CV experiments for estimating the redox diffusion coefficients for SOLVED, SAMs, and tetra(trimethylsiloxy)silane (TTMSS) coatings (Eq. 1).[65] TTMSS is a small siloxane present in the Sylgard 184 part A used for the PDMS SOLVED deposition. The CV studies on the TTMSS coated electrode were performed to compare the redox transport with electrodes coated with longer siloxane molecules and to evaluate the potential role of TTMSS in SOLVED film formation.

D~2.7×10^{-7} cm^2/s values for $Fe(CN)_6^{3-/4-}$ ions for the F-PDMS SOLVED and fluorinated-SAMs obtained using CV measurements were comparable but were ~16 times lower than the D values (~4.4×10^{-6} cm^2/s) for the TTMSS coated electrodes (Fig. 5c). The TTMSS coatings on glass also exhibited the water CA of ~90° with large standard deviations (±15°) between different spots on the same substrate. Significant larger I_{pc}' and lower water CA with large standard deviation for

the TTMSS coated electrodes suggested that, unlike SOLVED films, the TTMSS films possessed incomplete coverage and/or significant defects in them and that the SOLVED surfaces are unlikely to compose exclusively of TTMSS.

Although our CV studies implied similar I_{pc}, and diffusion coefficients for $Fe(CN)_6^{3-/4-}$ for both the SAMs and SOLVED films, there are some major physical differences exist between the SAMs and the SOLVED films. First, the hydrophobic part in the C_{18}-SAMs is highly ordered, whereas the SOLVED films were composed of less-ordered but much longer and possibly crosslinked chains. The thickness of the SOLVED films was ~3 times (~6.5 nm) that of C_{18}-SAM layer thickness (~2.2 nm). The larger film thickness and siloxane crosslinking in the SOLVED films yielded comparable water CA and CV responses with those of SAMs films.

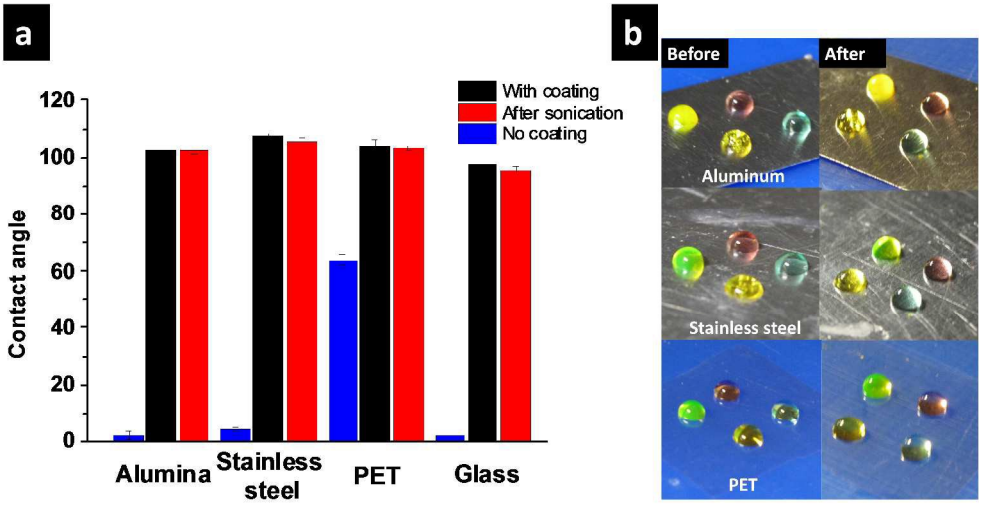

Figure 6. (a) The water CA of the PDMS SOLVED coated surfaces. Blue: original surfaces. Black: SOLVED coated surfaces. Red: sonicated SOLVED coated surfaces. (b) Colored dyes containing water droplets on aluminum, stainless steel, and PET substrates coated with the PDMS SOLVED before (left column) and after (right column) toluene sonication.

Proposed SOLVED mechanism on the surfaces. It is important to consider possible routes for vapor-phase SOLVED covalent binding of the siloxane polymers on various substrates (glass, silicon, aluminum, stainless stain, and PET, Fig. 6). Important questions need to consider are: what is/are the major chemical species involved in the SOLVED films on the surface? What is/are possible mechanism(s) for the formation of the siloxane films on the surfaces? Although glass, silicon, stainless steel, alumina, and PET were shown to possess siloxane films on their

surfaces, we use glass as a model surface for explaining the formation of the SOLVED on its surface. A similar mechanism should follow for other hydroxyl-containing surfaces the SOLVED. In our experiments, we used pure neat siloxane polymers (F-PDMS and N-PDMS) without initiator, crosslinker, or any other additives in the reaction. A commercial Sylgard 184 part A was used for the synthesis of PDMS SOLVED films (see TGA discussion in the SI). Scheme 2 shows a possible mechanism of covalent bound siloxane thin films using siloxane polymers. In step A, a glass substrate with ~4.9 OH/nm^2 [66] is heated to 150-250^{o}C during. The thermal treatment of glass resulted in desorption some water molecules (shown in blue ovals) from the surface.[67,68] Step B shows the covalently attached siloxanes films on the surface through a reaction between surface silanols and siloxane groups. The crosslinked SOLVED layers are shown by black lines joining two or more adjacent siloxane chains tethered to the surface. Step C shows the addition of siloxane layers to surface bound SOLVED layers with deposition time.

In the absence of possible sources of anions in our reaction vessels, we rule out SOLVED film formation through anion based siloxane-surface binding. Another potential reaction mechanism for SOLVED film formation in our experiments is through a radical mechanism. The potential radical sources for covalent linkage between the surface and siloxane polymers are singlet atomic oxygen and OH radicals. Singlet atomic O is produced through photolysis of air (O_2) whereas $^{\cdot}$OH is produced by a reaction between singlet atomic O and water.[69] We also ruled out photo-induced radical based siloxane-surface binding reaction mechanism because all the reactions in our SOLVED experiments were either performed in the glass vessels under inert atmosphere or in dark. Finally, the thermolytic dissociation of molecular water to $^{\cdot}$OH radicals is unlikely because Gibbs function becomes zero at temperature ~4700 K, thereby, ruling out radical formation through thermolysis under our experimental conditions.[70]

McCarthy proposed two water-assisted equilibration reactions between the surface silanols and siloxanes.[41] In the first reaction mechanism, the covalent surface-siloxane binding occurs by silanolysis of the PDMS chains by H^+ (from surface silanols of the substrate, pka~2-3[71]) followed by its condensation with the glass surface through nucleophilic attack by surface silanolate. The second reaction mechanism involves hydrolysis of PDMS to silanol-terminated siloxane polymer chains followed by covalent bonding between siloxane and surface silanols. The reaction mechanisms proposed by McCarthy are still operative in our studies. However, the

previous reported studies involve the siloxane polymer fluids in contact with the surfaces[41,42] whereas the vapor-phase reaction with the surface is operative in the present experiments. Further, the activated oligomers in the vapor phase (orange lines, step D in Scheme 2) can be covalently bound to surface bound siloxane chains (blue lines in Scheme 2). The attachment of oligomers/monomers to already covalently bound (blue lines in Scheme 2) molecules on the surface can explain the observed increase in the film thickness and/or the surface coverage (in x-y plane). Although it is not possible to predict and differentiate with high confidence which, if any, between these two processes (i.e., increase in x-y surface coverage and/or z-axial film thickness with deposition time), we expect that both of these routes are operative in the deposition process. Further, because the silanol/siloxane reactions involved in the SOLVED process are believed to be non-discriminatory in nature, the linkages between SOLVED siloxane chains and the surface silanols are potentially through a single or multiple contact spots (blue lines, step D in Scheme 2). Larger siloxane chains may bound through two or multiple-covalent contacts with the surface whereas the shorter oligomers may prefer single-covalent contact with the substrate surface.[42] Finally, the crosslinking within SOLVED is evident from our XPS data (grey lines, Scheme 2).

Finally, we comment on the incorporation of cyclic siloxane with the SOLVED films. Our FTIR experimental data indicated the SOLVED films were dominantly containing linear siloxanes (1107 cm^{-1} peak) on the surface, but the cyclic siloxane content (1011 cm^{-1} peak) in the SOLVED coating films was minor (Fig. 1S). The thermal degradation of siloxane polymer chains to cyclic siloxane oligomers (D_3 and D_4) and small linear chain fragments in the vapor phase[72] is assumed to be a possible source of cyclic siloxanes in the SOLVED films (Step D in Scheme 2). The depolymerization of PDMS is thought to be dominated by the molecular structure (i.e. Si-O bonds) and kinetic considerations rather than controlled through thermodynamics where the dissociation of stronger Si-O bonds (bond energy ~106 kcal/mol) rather than those of weaker Si-C bonds (bond energy ~78 kcal/mol) is implicated in the formation of degradation products in PDMS.[72] For the low degradation temperature range (<400 ^{o}C) and slow heating conditions are known to involve molecular splitting of the loop conformations within flexible PDMS chains along with contributions from empty silicon d-orbitals. These thermal treatment generally yield predominantly hexamethylcyclotrisiloxane (D_3) and octamethylcyclotetrasiloxane (D_4) and a small amount of linear fragments.[72]

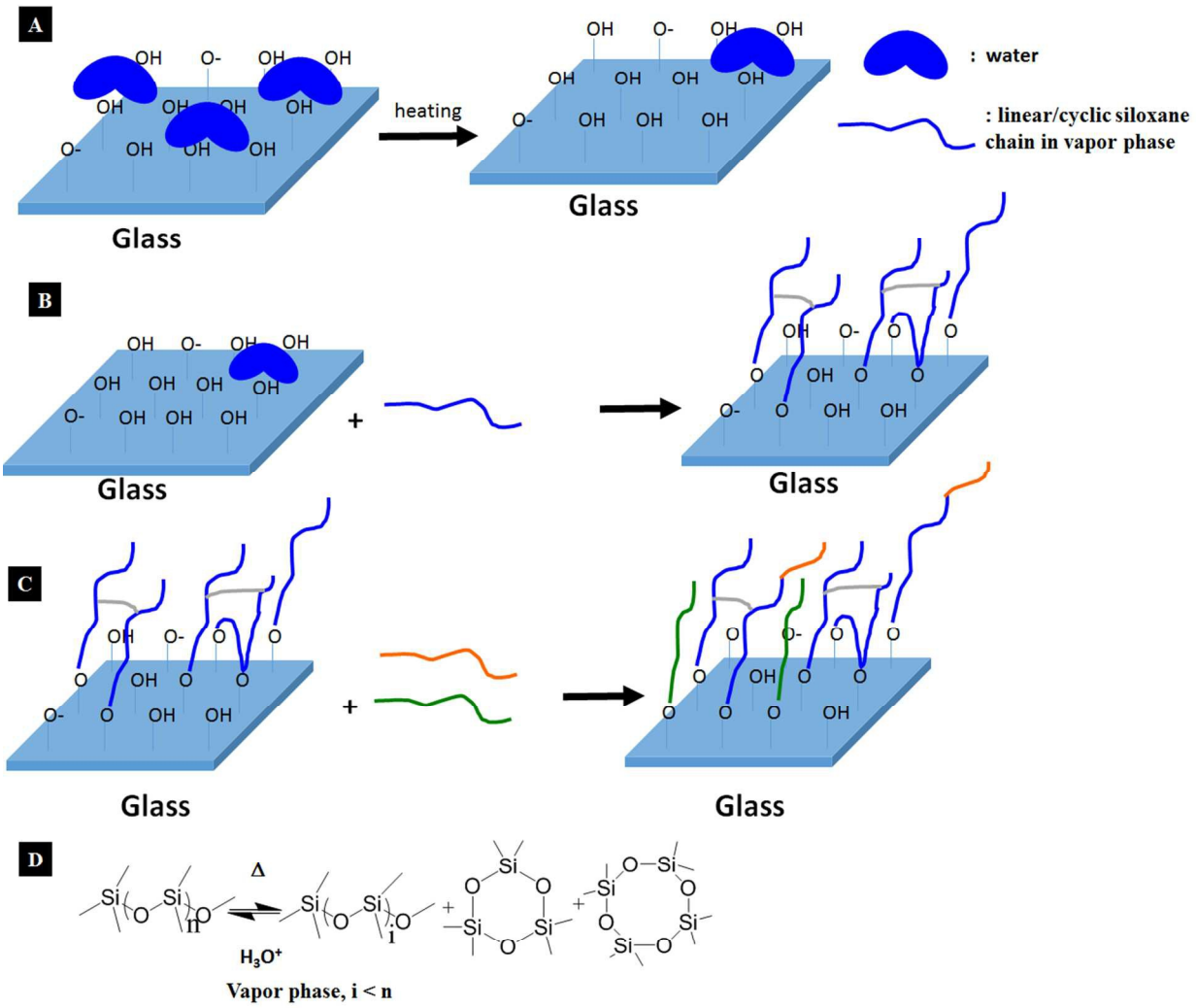

Scheme 2. A proposed mechanism of vapor-phase covalent bound siloxane films on glass surfaces.

Comments on SOLVED mechanism on aluminum, steel, and PET. We have not investigated in detail the SOLVED mechanism on the other three surfaces (stainless steel, aluminum, and PET). However, there are numbers of literature reports that the thermal oxidized layers are formed on those surfaces. For a stainless steel surface, a native oxide layer ~ a few nm thick was observed[73,74] and hydroxyl groups were detected on the surface during heating in the air.[75] For an aluminum surface, a native oxide layer ~0.5-1 nm was observed on clean aluminum surface.[76] The oxide surface will be hydrated by water molecules chemisorb on it providing hydroxyl groups on the surface.[77] The SOLVED mechanism on the PET surfaces is less clear at this point. The thermal treatment of the PET produces highly reactive species including free radicals, peroxy, and hydroperoxide.[78] The generated highly reactive species potentially react with the

siloxane chains allowing covalent binding of the activated chains on the surface. However, a detailed study is needed to fully understand the covalently bonding of the silioxanes on the PET surfaces. Overall, we believe that the hydroxyl-groups at the various surfaces are involved in the covalent-bonding of the siloxanes.

Self-limiting thickness for SOLVED. Another interesting observation in our experiments is self-limiting thickness (~6.5 nm) of the PDMS SOLVED. This observation suggests that the reaction of the siloxane with the surface may involve siloxane-surface silanol equilibrium in agreement with the previous studies.[41,42] The molecular weight dependence of the siloxane on the film thickness suggested that the equilibrium of the siloxane-surface reaction is slow relative to equilibration of the surface silanol groups.[41] At higher deposition temperature (>200 ^{o}C), another equilibrium reaction between linear siloxane and cyclic siloxane is also expected in the reaction atmosphere. These two equilibria reactions are believed to play a role in the self-limiting film thickness of the siloxane-surface covalent equilibration. The studies involving in-situ ellipsometry and FTIR, solid-state NMR, and angle-resolved XPS studies may provide further crucial information on the chemical nature, reaction mechanism, and self-limiting film thickness.

Role of water in the formation of the SOLVED films. Considering the most apparent activation energy of ~11 kcal/mol for the vapor-phase PDMS-SOLVED reaction, a reasonable question: "*why are the vapor-phase SOLVED-like films not reported in the literature?*" needs some thoughts. The simplest answer is that this reaction may have been observed by researchers but was ignored. More importantly, the insulator surfaces contain a thin adlayer of water.[79] For example, at 50% relative humidity (RH) ~0.4 nm and 1 nm thick water layer is present Al(0001) and mica surfaces respectively,[79] whereas the SiO_2 surface (similar in surface chemistry to amorphous glass) contains 0.6 nm (~2 two layers) to >2 nm (~6 layers) thick water film depending upon the RH.[80] Moreover, the condensation of water on mica is exothermic at all the coverages. The enthalpy and entropy values for water condensation on the mica surface are in 40-54 kcal/mol and 40-100 J/mol K range respectively.[79] Large enthalpy values for water adhered on the insulated surfaces suggest that the water molecules are bound strongly to the insulated surfaces and that the surface may remain covered with water at temperature >100^{o}C. Indeed, the heating of the surfaces to temperature >100^{o}C is usually needed to desorb the bound water from the glass and Si wafers. For the SOLVED experiments performed at temperatures

≤100°C, a water barrier layer is believed to play a crucial role in protecting the surface from being reacted with the siloxane molecules. The previous reported studies on liquid siloxane in

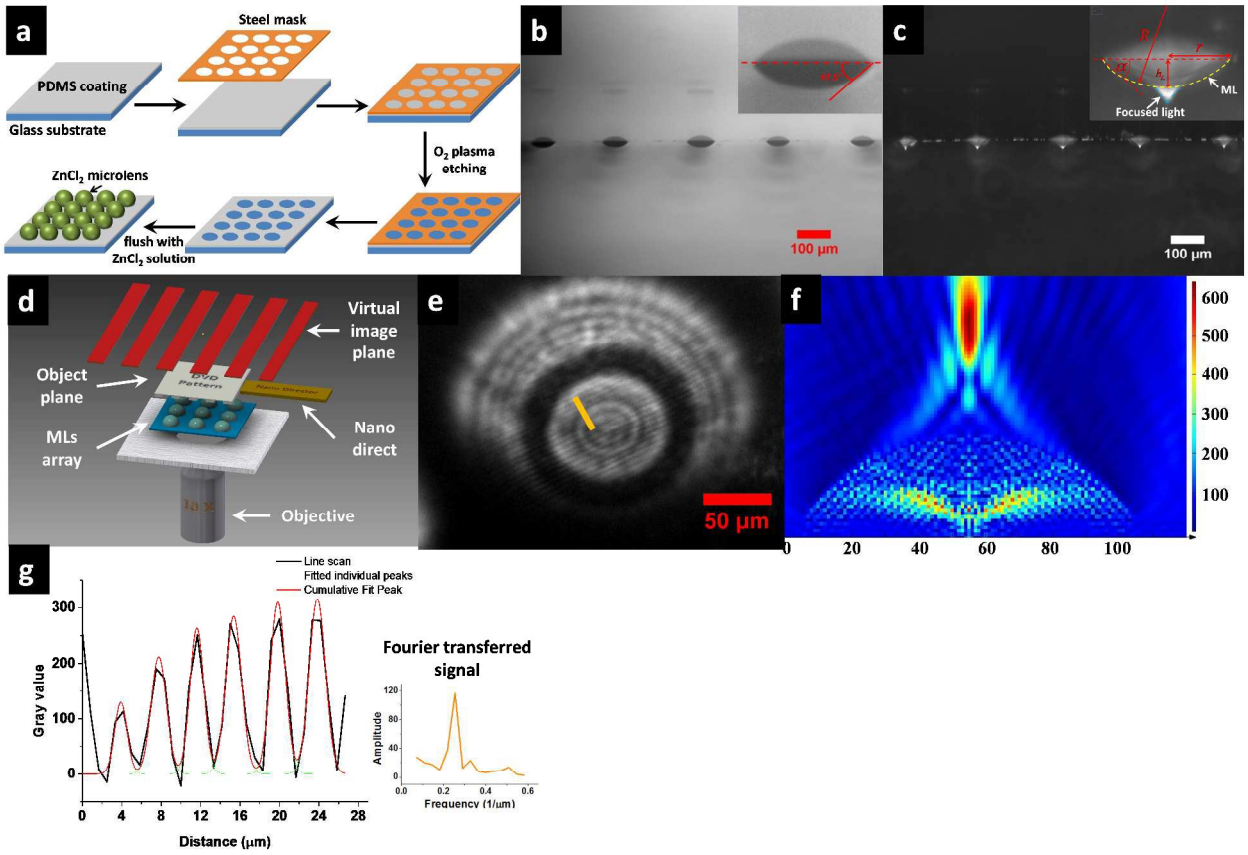

Figure 7. Enhanced resolution imaging using MLs fabricated on the SOLVED coating glass substrate. (a) Scheme for the fabrication of self-assembled $ZnCl_2$ MLs array on a SOLVED coated glass substrate. (b) A bright-field micrograph of the $ZnCl_2$ MLs array prepared on the SOLVED coatings. Inset in (b) shows the water CA of single MLs on patterned PDMS coated glass surface. (c) A dark-field micrograph of the same MLs in (a) showing focusing through MLs. Inset in (c) shows focusing of light though a single ML. (d) Set up used for the high-resolution near-field imaging. (e) A magnified bright-field image of the DVD patterns using a single ML in near-field imaging modes. (f) FDTD analysis for single $ZnCl_2$ MLs in an array fabricated on patterned PDMS SOLVED coating on a glass slide. Light source was a total field scatter field (TFSF) with incident light intensity of 30 units. The mesh sizes for FDTD calculations and wavelength excitation (λ_{ex}) were 250 nm and 580 nm respectively. (g) Line scan of the resolved patterns in (e). The inset in (g) is fourier transformation of the line scan data in (e). Scale bars in (b), (c), and (e) are 100 μm, 100 μm, and 50 μm respectively.

contact with surfaces showed complete coverage at 100°C after 24 hours reaction time.[42] Importantly, in these studies, the concentration of the siloxane in contact with the surface is ≈ 0.015 mM (assuming the molecular weight (M_w) of the siloxane was 60 kD) which is expected to be significantly higher than in our deposition studies (see below). The SOLVED studies involve siloxane molecules in the vapor phase react with the surface silanol groups. Under these conditions, the concentration of the siloxanes in contact with the surface silanol depends upon the water solubility and vapor pressure of the siloxane. The water solubility of the PDMS (M_w~60kD) used in our studies is 0.076 ppm[54] suggesting that water barrier layer will reduce the concentration of siloxanes at the substrate-water interface. Finally, the vapor pressure of the siloxane polymers needs to be taken in account because our deposition requires the molecules present in the vapor to react with the surface. The reported vapor pressure of tetracosamethylundecasiloxane (M_w~830 D) is ~3.5 x 10^{-7} Pa [81] (398 K<T<439). Because the molecular weight of the siloxanes used in our studies >60 times larger than tetracosamethylundecasiloxane, we infer that the vapor pressure of our siloxanes is much smaller than that of tetracosamethylundecasiloxane. This means that the siloxane molecule concentration in the vapor phase is small under our experimental conditions. Overall, the presence of the water molecules on the substrate surface, and reduced siloxane concentration in the vapor phase due to low vapor pressure, high molecular weight, and reduced solubility in water reduced the access of siloxanes to the surface, thereby, contributing to incomplete surface coverage at the lower temperature (<100 °C) experiments.

Microlens (MLs) array fabrication and super-high resolution imaging. Previous work in the literature has shown that the MLs can significantly improve the optical spatial resolution.[82,83] Recently, the fabrication of the MLs based on the polar electric crystal[84], lithography,[85] and liquid crystals[86] are reported. We utilized the SOLVED functionalized surfaces for the fabrication of aqueous ML array for near-field imaging applications (see SI). Fig. 7a shows a scheme of fabricating MLs array on a SOLVED coated glass cover slip. Following oxygen etching through a stainless steel mesh with a pore diameter of ~150 μm, aqueous $ZnCl_2$ (refractive index 1.57) MLs were formed by flushing the plasma-treated surface with $ZnCl_2$ solution (Figs. 7b and 11S). A DVD specimen containing an array of grooves with a periodicity of ~640 nm was attached on a xyz-piezoelectric stage (Fig. 7d). The z-piezoelectric stage was crucial to precisely control the specimen-ML distance (l) ~300 nm for near-field optical imaging.

The near-field optical imaging means that $l<\lambda_{incident}$, where $\lambda_{incident}$ is the wavelength used for excitation.During imaging process, the incident light was focused through each ML on to the specimen, and a virtual image magnified by the microscope was captured by a CCD camera (Fig. 7e). We have characterized MLs using optical microscopy and also performed Finite-difference-time-domain (FDTD) calculations as well (Fig. 7f). The bright- and dark-field optical micrographs of the multiple MLs on a SOLVED-coated glass substrate are shown in Figs. 8a and 8b respectively. The focusing of light through multiple rows of MLs is also available in the movie M1 (see SI). The water micro-contact angle of the MLs on fabricated the SOLVED surface was ~47.5° (inset of Fig. 7b) which is smaller than water CA observed on the SOLVED surfaces. The decrease in the water CA for the MLs is attributed to plasma etching of the surface without a sharp hydrophilic-hydrophobic boundary. The focal length (f) of a plano-convex refractive ML was estimated using geometric optics analysis:[87]

$$f = \frac{h_L + r^2 / h_L}{2(n-1)} \qquad \text{Eq. 2}$$

where h_L, r, and $n(\lambda)$ are average height, average lens radius, and the refractive index of the ML respectively. For an ML with r = 40 μm, h_L = 20 μm, and n~1.57 for a saturated $ZnCl_2$ solution, the estimated f is ~93 μm. Our experimental data shows that the light was focused though MLs ~27 μm from the surface of the ML (Fig. 7c inset). That is, the experimental f is ~(45+27)=72 μm. The FDTD calculations provide an accurate analysis of electromagnetic field interaction with matter. Our FDTD calculations for the focusing of the light through two $ZnCl_2$ plano-convex MLs (r=40 μm) is shown in Fig. 7f. The highest and lowest electric field (E) of the electromagnetic wave in space are shown in the brown and dark blue colors respectively (Fig. 7f). The highest E value was found at ~24 μm away from the ML vertex, yielding f~64 μm. This is in agreement with our experimental f=72 μm. f=93 μm obtained using calculations based on the geometric optics overestimate f because of many assumptions involved in the derivation of the Eq. 2. $|E|$ at the focal point of ML was ~600 units which is ~20 times stronger than that for incident light (set as 30 units). Because $I \propto |E|^2$, the light intensity (I) at the focal point was ~400 times larger than the incident intensity (Fig. 7f). M2 (bright field) and M3 (dark field) showing focusing of light using multiple rows of MLs in the bright- and dark-fields respectively are available in the supplementary document.

A tungsten-halogen lamp with radiation wavelength maxima ($\lambda_{incident}$) ~600 nm was used for illumination of the sample. The diffraction limited resolution ($r = \frac{\lambda_{incident}}{2NA}$) of our microscope with a 10x objective with a numerical aperture (*NA*) ~0.25 is ~1200 nm.[88] That means that the DVD features with a periodicity of 640 nm cannot be resolved using a wide-field conventional microscope that utilized an *NA*~0.25. Fig. 7e clearly shows the resolved DVD patterning with the described set up using an ML. A line scan showing a sinusoidal curve (periodical peaks and valleys) for the ML-resolved image is shown in the Fig. 7g. Fourier-transformed data of the line scan yielded a peak at 0.25 μm^{-1} that corresponds to a pitch of 4 μm for the patterns resolved using an aqueous ML. The magnification (*M*) for the ML-resolved image was ~6.6 (Fig. 7g, inset). *M* is defined as the ratio of the periodicity in the resolved optical image to that of the periodicity in the SEM image. These experiments demonstrate that the use SOLVED films for the formation of aqueous MLs yielded enhanced resolution compared to a conventional wide-field microscope in the near-field imaging. Apart from near-field imaging, the SOLVED coatings can also provide an alternative to functional nanoscale coatings for many potential applications in materials, alternative-energy, pharmaceutical, life- and biological sciences.

We now discuss the general implications of the SOLVED for the surface functionalization and contamination, and the materials consideration for the SOLVED coatings.

Implications of the SOLVED to surface decoration. The SOLVED process described here is an environmental-friendly and solvent-free one step deposition process which can be scaled up both in batch and continuous processes. For example, through the use of a continuous conveyer oven, the substrates can be sprayed with siloxane polymers/oligomers of different functionality, for example, fluoro-, amino-, cyano-siloxanes, while moving through the oven. This may allow continuous coating of the surfaces with SOLVED (please see SI for more details).

Implication of the SOLVED films to siloxane contamination of the surfaces. Based on our experimental results, the chemical reaction of siloxanes with the surfaces can result in unintended surface contamination. The surface coverage of siloxane molecules in the SOLVED depends upon the concentration of the vapor-phase siloxane molecules in the vicinity of the surface and temperature of the surface (see above). Higher temperature will increase the siloxane concentration in close proximity to the surfaces and will also desorb the adlayer of the water on the surfaces, thereby, enhancing the kinetics and surface coverage of the SOLVED.

The siloxane coatings will result changes in the surface functionality and morphology. The cleaning of the SOLVED coated surfaces may require piranha or ozone based oxidative cleaning that removes the hydrophobic alkyl portion of the SOLVED coating. However, the covalently bound Si-O backbone polymer chains may survive these oxidative cleaning processes. More severe KOH bath treatment or etching using SF_6 or CF_4 (or other fluorine containing molecules) plasma may be needed for a complete removal of the SOLVED-like coatings.

Material considerations for the SOLVED and SAMs coatings. The starting materials for the SOLVED coatings are siloxane polymers (pre-polymers) that are usually less expensive than many silanes of similar functionality. The silanes are usually hydrolytically less stable than siloxane polymers. Thus, whereas many silanes require inert atmosphere for their storage, the siloxane polymers can be usually stored under ambient conditions for extended period of time without significant deterioration. With comparable water CA and photostability for SOLVED and SAMs coatings, the SOLVED are potential alternative to some silanes.

Conclusion. We demonstrate a simple and facile method of covalent-bound siloxane films of a few nanometers thick on surfaces. The SOLVED deposition was accomplished by heating commercially-available functional siloxane homo- and co-polymers to ~100-250°C in the vicinity of a surface. The water CA of the functionalized SOLVED surfaces was tuned over a wide range (~30^o-97^o) using oxygen plasma treatment. Our FTIR, MS, and XPS data indicated that the SOLVED films retained the primarily chemical nature of the polymers used for functionalization of the surface coating but some oxidation of the films was also evident in the optical spectroscopic measurements. Possible mechanisms for the covalent binding of the siloxanes on the surfaces were also discussed. Through selective patterning of the SOLVED surfaces, an array of aqueous MLs was fabricated process on the SOLVED surfaces. ML fabricated on SOLVED surfaces was used for imaging in the near-field regime which yielded higher spatial resolution than that was achievable by a conventional wide-field microscope. The facile and solvent-free synthesis of the optical transparent functional SOLVED coatings may provide many potential applications. For example, with appropriate choice of siloxane polymers for the surface functionalization, the SOLVED possesses potential applications in protecting and lubricating surfaces; micro-fluidics, optics, and micro-electronics device fabrication; and in biology and life sciences.

Acknowledgements. We acknowledge National Science Foundation (CHE-0748676 and CHE-0959568), National Institutes of Health (GM 106364 and GM 080711), and the Office of Vice-Chancellor of Research (OVCR) at the SIUC for the partial financial support. We thank Profs. Kyle Plunkett, Samir Aouadi, and Colleen Scott for the use of their CV, ellipsometry, and FTIR instruments respectively. We also acknowledge assistance from Dr. Mary Kinsel for assisting us in mass spectrometry.

Supplementary Information

Supplementary information containing Figs. 1-9, Schemes 1S, Tables 1S-3S, and movies M1-M3 is available free of charge.

References

(1) Nitzan, B.; Margel, S. *Journal of Polymer Science Part A: Polymer Chemistry* **1997**, *35*, 171.
(2) Bigelow, W. C.; Pickett, D. L.; Zisman, W. A. *Journal of Colloid Science* **1946**, *1*, 513.
(3) Allara, D. L.; Nuzzo, R. G. *Langmuir* **1985**, *1*, 45.
(4) Allara, D. L.; Nuzzo, R. G. *Langmuir* **1985**, *1*, 52.
(5) Nuzzo, R. G.; Allara, D. L. *Journal of the American Chemical Society* **1983**, *105*, 4481.
(6) Troughton, E. B.; Bain, C. D.; Whitesides, G. M.; Nuzzo, R. G.; Allara, D. L.; Porter, M. D. *Langmuir* **1988**, *4*, 365.
(7) Ulman, A. *Chem. Rev.* **1996**, *96*, 1533.
(8) Tian, Y.; Su, B.; Jiang, L. *Advanced Materials* **2014**, *26*, 6872.
(9) Liu, M.; Wang, S.; Wei, Z.; Song, Y.; Jiang, L. *Advanced Materials* **2009**, *21*, 665.
(10) Tuteja, A.; Choi, W.; Ma, M.; Mabry, J. M.; Mazzella, S. A.; Rutledge, G. C.; McKinley, G. H.; Cohen, R. E. *Science* **2007**, *318*, 1618.
(11) Tuukka Verho , C. B., Piers Andrew , Sami Franssila , Olli Ikkala , and Robin H. A. Ras *Advanced Materials* **2010**, 6.
(12) Chen, H.-Y.; Elkasabi, Y.; Lahann, J. *Journal of the American Chemical Society* **2006**, *128*, 374.
(13) Prakash, S.; Long, T. M.; Selby, J. C.; Moore, J. S.; Shannon, M. A. *Analytical Chemistry* **2007**, *79*, 1661.
(14) Moon, H.; Seong, H.; Shin, W. C.; Park, W.-T.; Kim, M.; Lee, S.; Bong, J. H.; Noh, Y.-Y.; Cho, B. J.; Yoo, S.; Im, S. G. *Nat Mater* **2015**, *14*, 628.
(15) Zhang, Y.; Zhang, L.; Zhou, C. *Accounts of Chemical Research* **2013**, *46*, 2329.
(16) Wu, K. H.; Chao, C. M.; Yeh, T. F.; Chang, T. C. *Surface and Coatings Technology* **2007**, *201*, 5782.
(17) Chrysi Kapridaki, P. M.-K. *Progress in Organic Coatings* **2012**, 11.
(18) Garima Verma, S. K. D., A.S. Khanna *Surface & Coatings Technology* **2012**, *212*, 8.
(19) Li, H.; Wang, J.; Yang, L.; Song, Y. *Adv. Funct. Mater.* **2008**, *18*, 3258.
(20) Su, B.; Wang, S.; Ma, J.; Song, Y.; Jiang, L. *Adv. Funct. Mater.* **2011**, *21*, 3297.
(21) Su, B.; Wang, S.; Wu, Y.; Chen, X.; Song, Y.; Jiang, L. *Advanced Materials (Weinheim, Germany)* **2012**, *24*, 2780.
(22) Helander, M. G.; Wang, Z. B.; Qiu, J.; Greiner, M. T.; Puzzo, D. P.; Liu, Z. W.; Lu, Z. H. *Science* **2011**, *332*, 944.

(23) Deng, X.; Nie, R.; Li, A.; Wei, H.; Zheng, S.; Huang, W.; Mo, Y.; Su, Y.; Wang, Q.; Li, Y.; Tang, J.; Xu, J.; Wong, K.-y. *Advanced Materials Interfaces* **2014**, *1*, n/a.

(24) Li, A.; Nie, R.; Deng, X.; Wei, H.; Zheng, S.; Li, Y.; Tang, J.; Wong, K.-Y. *Applied Physics Letters* **2014**, *104*, 123303.

(25) Nie, R.; Li, A.; Deng, X. *Journal of Materials Chemistry A* **2014**, *2*, 6734.

(26) Jung, Y. C.; Bhushan, B. *ACS Nano* **2009**, *3*, 9.

(27) Jin Yang, Z. Z., Xuehu Mena, Xianghui Xu *Applied Surface Science* **2009**, *255*, 4.

(28) Jiang, B. F. X. a. L. *Advanced Materials* **2008**, *20*, 2858.

(29) Li, M.; Zhai, J.; Liu, H.; Song, Y.; Jiang, L.; Zhu, D. *Journal of Physical Chemistry B* **2003**, *107*, 9954.

(30) Mine, E.; Yamada, A.; Kobayashi, Y.; Konno, M.; Liz-Marzán, L. M. *Journal of Colloid and Interface Science* **2003**, *264*, 385.

(31) Vidic, J.; Pla-Roca, M.; Grosclaude, J.; Persuy, M.-A.; Monnerie, R.; Caballero, D.; Errachid, A.; Hou, Y.; Jaffrezic-Renault, N.; Salesse, R.; Pajot-Augy, E.; Samitier, J. *Analytical Chemistry* **2007**, *79*, 3280.

(32) Chan, C. M.; Ko, T. M.; Hiraoka, H. *Surface Science Reports* **1996**, *24*, 1.

(33) Sperling, R. A.; Parak, W. J. *Philosophical Transactions of the Royal Society of London A: Mathematical, Physical and Engineering Sciences* **2010**, *368*, 1333.

(34) Goddard, J. M.; Hotchkiss, J. H. *Progress in Polymer Science* **2007**, *32*, 698.

(35) Tada, H.; Nagayama, H. *Langmuir* **1995**, *11*, 136.

(36) Howarter, J. A.; Youngblood, J. P. *Langmuir* **2006**, *22*, 11142.

(37) Britt, D. W.; Hlady, V. *Journal of colloid and interface science* **1996**, *178*, 775.

(38) Krasnoslobodtsev, A. V.; Smirnov, S. N. *Langmuir* **2002**, *18*, 3181.

(39) McGovern, M. E.; Kallury, K. M. R.; Thompson, M. *Langmuir* **1994**, *10*, 3607.

(40) Zheng, P.; McCarthy, T. J. *Langmuir* **2010**, *26*, 18585.

(41) Krumpfer, J. W.; McCarthy, T. J. *Langmuir* **2011**, *27*, 11514.

(42) Graffius, G.; Bernardoni, F.; Fadeev, A. Y. *Langmuir* **2014**, *30*, 14797.

(43) Yu-Fu, L.; Yong-Xia, X.; Dong-Peng, X.; Guang-Liang, L. *Journal of Polymer Science: Polymer Chemistry Edition* **1981**, *19*, 3069.

(44) Litvinov, V.; Barthel, H.; Weis, J. *Macromolecules* **2002**, *35*, 4356.

(45) Krumpfer, J. W.; McCarthy, T. J. *Langmuir* **2011**, *27*, 11514.

(46) Thibault, C.; Séverac, C.; Mingotaud, A.-F.; Vieu, C.; Mauzac, M. *Langmuir* **2007**, *23*, 10706.

(47) Wang, X.; Östblom, M.; Johansson, T.; Inganäs, O. *Thin Solid Films* **2004**, *449*, 125.

(48) Yang, L.; Shirahata, N.; Saini, G.; Zhang, F.; Pei, L.; Asplund, M. C.; Kurth, D. G.; Ariga, K.; Sautter, K.; Nakanishi, T.; Smentkowski, V.; Linford, M. R. *Langmuir* **2009**, *25*, 5674.

(49) Chae, S. S.; Oh, J. Y.; Park, J. H.; Choi, W. J.; Han, J. H.; Lee, J.-O.; Baik, H. K.; Lee, T. I. *Chemical Communications* **2015**, *51*, 5844.

(50) Lin, Y.; Wang, L.; Krumpfer, J. W.; Watkins, J. J.; McCarthy, T. J. *Langmuir* **2013**, *29*, 1329.

(51) Tsougeni, K.; Tserepi, A.; Gogolides, E. *Microelectronic Engineering* **2007**, *84*, 1104.

(52) Lee, J. N.; Park, C.; Whitesides, G. M. *Analytical Chemistry* **2003**, *75*, 6544.

(53) Girard, O.; Cohen-Addad, J. P. *Polymer* **1991**, *32*, 860.

(54) Mark, J. E., ed. . New York, NY: Oxford University Press. **1999**.

(55) Murthy, S. K.; Olsen, B. D.; Gleason, K. K. *Langmuir* **2002**, *18*, 6424.

(56) O'Shaughnessy, W. S.; Gao, M. L.; Gleason, K. K. *Langmuir* **2006**, *22*, 7021.

(57) Reeja-Jayan, B.; Chen, N.; Lau, J.; Kattirtzi, J. A.; Moni, P.; Liu, A.; Miller, I. G.; Kayser, R.; Willard, A. P.; Dunn, B.; Gleason, K. K. *Macromolecules* **2015**, *48*, 5222.

(58) Camino, G.; Lomakin, S. M.; Lageard, M. *Polymer* **2002**, *43*, 2011.

(59) Bowden, N.; Huck, W. T. S.; Paul, K. E.; Whitesides, G. M. *Applied Physics Letters* **1999**, *75*, 2557.
(60) O'Hare, L.-A.; Parbhoo, B.; Leadley, S. R. *Surface and Interface Analysis* **2004**, *36*, 1427.
(61) Dong, X.; Gusev, A.; Hercules, D. M. *Journal of the American Society for Mass Spectrometry* **1998**, *9*, 292.
(62) Dickson, J. L.; Gupta, G.; Horozov, T. S.; Binks, B. P.; Johnston, K. P. *Langmuir* **2006**, *22*, 2161.
(63) Emami, F. S.; Puddu, V.; Berry, R. J.; Varshney, V.; Patwardhan, S. V.; Perry, C. C.; Heinz, H. *Chemistry of Materials* **2014**, *26*, 2647.
(64) Chen, C.; Zhang, N.; Li, W.; Song, Y. *Environmental Science & Technology* **2015**, *49*, 14680.
(65) Faukner, A. J. B. a. L. R. *Electrochemical Methods: Fundamental and Applications* Second ed.; John Wiley & Sons: New York, 2001.
(66) Zhuravlev, L. T. *Colloids and Surfaces A: Physicochemical and Engineering Aspects* **2000**, *173*, 1.
(67) Tuzi, Y. *Journal of the Physical Society of Japan* **1962**, *17*, 218.
(68) Nishioka, G. M. *Journal of Non-Crystalline Solids* **1990**, *120*, 34.
(69) Bernardini, C.; Stoyanov, S. D.; Cohen Stuart, M. A.; Arnaudov, L. N.; Leermakers, F. A. M. *Langmuir* **2011**, *27*, 2501.
(70) E. Funk, J. *International Journal of Hydrogen Energy* **2001**, *26*, 185.
(71) Lewis, J. A. *Journal of the American Ceramic Society* **2000**, *83*, 2341.
(72) Camino, G.; Lomakin, S. M.; Lazzari, M. *Polymer* **2001**, *42*, 2395.
(73) Tardio, S.; Abel, M.-L.; Carr, R. H.; Castle, J. E.; Watts, J. F. *Journal of Vacuum Science & Technology A* **2015**, *33*, 05E122.
(74) Sánchez-Tovar, R.; Leiva-García, R.; García-Antón, J. *Thin Solid Films* **2015**, *576*, 1.
(75) Jussila, P.; Ali-Löytty, H.; Lahtonen, K.; Hirsimäki, M.; Valden, M. *Surface and Interface Analysis* **2010**, *42*, 157.
(76) Evertsson, J.; Bertram, F.; Zhang, F.; Rullik, L.; Merte, L. R.; Shipilin, M.; Soldemo, M.; Ahmadi, S.; Vinogradov, N.; Carlà, F.; Weissenrieder, J.; Göthelid, M.; Pan, J.; Mikkelsen, A.; Nilsson, J. O.; Lundgren, E. *Applied Surface Science* **2015**, *349*, 826.
(77) Padhye, R.; Aquino, A. J. A.; Tunega, D.; Pantoya, M. L. *ACS Applied Materials & Interfaces* **2016**, *8*, 13926.
(78) Peterson, J. D.; Vyazovkin, S.; Wight, C. A. *Macromolecular Chemistry and Physics* **2001**, *202*, 775.
(79) Ewing, G. E. *Chemical Reviews* **2006**, *106*, 1511.
(80) Verdaguer, A.; Weis, C.; Oncins, G.; Ketteler, G.; Bluhm, H.; Salmeron, M. *Langmuir* **2007**, *23*, 9699.
(81) Lei, Y. D.; Wania, F.; Mathers, D. *Journal of Chemical & Engineering Data* **2010**, *55*, 5868.
(82) Darafsheh, A.; Walsh, G. F.; Dal Negro, L.; Astratov, V. N. *Applied Physics Letters* **2012**, *101*, 141128.
(83) Lee, J. Y.; Hong, B. H.; Kim, W. Y.; Min, S. K.; Kim, Y.; Jouravlev, M. V.; Bose, R.; Kim, K. S.; Hwang, I.-C.; Kaufman, L. J.; Wong, C. W.; Kim, P.; Kim, K. S. *Nature* **2009**, *460*, 498.
(84) Grilli, S.; Miccio, L.; Vespini, V.; Finizio, A.; De Nicola, S.; Ferraro, P. *Opt. Express* **2008**, *16*, 8084.
(85) Dong, L.; Agarwal, A. K.; Beebe, D. J.; Jiang, H. *Advanced Materials* **2007**, *19*, 401.
(86) Ren, H.; Fan, Y.-H.; Gauza, S.; Wu, S.-T. *Optics Communications* **2004**, *230*, 267.
(87) Ph, N.; Völkel, R.; Herzig, H. P.; Eisner, M.; Haselbeck, S. *Pure and Applied Optics: Journal of the European Optical Society Part A* **1997**, *6*, 617.
(88) Heintzmann, R.; Ficz, G. *Briefings in Functional Genomics & Proteomics* **2006**, *5*, 289.